Optimal fine-scale structures in compliance minimization for a uniaxial load*

Robert V. Kohn† and Benedikt Wirth‡

June 2, 2014

Abstract

We consider the optimization of the topology and geometry of an elastic structure $\mathcal{O} \subset \mathbb{R}^2$ subjected to a fixed boundary load, i. e. we aim to minimize a weighted sum of material volume $\mathrm{Vol}(\mathcal{O})$, structure perimeter $\mathrm{Per}(\mathcal{O})$, and structure compliance $\mathrm{Comp}(\mathcal{O})$ (which is the work done by the load). As a first simple and instructive case, this article treats the situation of an imposed uniform uniaxial tension load in 2D. If the weight ε of the perimeter is small, optimal geometries exhibit very fine-scale structure which cannot be resolved by numerical optimization. Instead, we prove how the minimum energy scales in ε, which involves the construction of a family of near-optimal geometries and thus provides qualitative insights. The construction is based on a classical branching procedure with some features unique to compliance minimization. The proof of the energy scaling also requires an ansatz-independent lower bound, which we derive once via a classical convex duality argument (which is restricted to 2D and the uniaxial load) and once via a Fourier-based refinement of the Hashin–Shtrikman bounds for the effective elastic moduli of composite materials. We also highlight the close relation to and the differences from shape optimization with a scalar PDE-constraint, and a link to the pattern formation observed in intermediate states of type-I superconductors.

1 Problem formulation and discussion

The aim of this article is to gain some insight into optimal geometries of elastically loaded structures, that is, geometries which achieve an optimal balance between some measure of structural rigidity, material weight, and structural complexity. We here consider the case where structural rigidity and complexity

*RVK gratefully acknowledges support from NSF through grants DMS-0807347 and OISE-0967140. BW gratefully acknowledges the support of a Courant Instructorship during which this work was begun.

†Courant Institute of Mathematical Sciences, New York University, 251 Mercer Street, New York 10012, USA, kohn@cims.nyu.edu

‡Institute for Numerical and Applied Mathematics, University of Münster, Einsteinstraße 62, 48159 Münster, Germany, Benedikt.Wirth@uni-muenster.de

are expressed in terms of the elastic compliance and the geometry perimeter, respectively. If a low structural complexity or equivalently a small perimeter is of minor importance, optimal geometries often exhibit very fine microstructure, which is difficult to capture by numerical optimization. However, following the lead by Kohn and Müller [18], one can achieve some understanding by exploring how the energy of optimal geometries scales in the model parameters. Such an analysis involves constructing a family of geometries with a certain scaling and proving that no other construction can do better. As a first instructive case we focus here on two spatial dimensions and a simple geometry with an imposed uniaxial load.

1.1 Introduction to compliance minimization

The elastic compliance of a structure $\mathcal{O} \subset \mathbb{R}^2$ subjected to a surface load $F : \Gamma \to \mathbb{R}^2$ on a part of the boundary $\Gamma \subset \partial\mathcal{O}$ is defined as

$$\mathrm{Comp}(\mathcal{O}) = \frac{1}{2}\int_\Gamma F \cdot u \,\mathrm{d}a$$

for the equilibrium displacement $u : \mathcal{O} \to \mathbb{R}^2$, which is the minimizer of the free energy [13]

$$\mathrm{E}[u] = \int_{\mathcal{O}} \frac{1}{2} C\epsilon(u) : \epsilon(u) \,\mathrm{d}x - \int_\Gamma F \cdot u \,\mathrm{d}a \quad \text{with } \epsilon(u) = \frac{1}{2}(\nabla u + \nabla u^T)\,,$$

potentially subject to some Dirichlet boundary conditions on part of $\partial\mathcal{O} \setminus \Gamma$. Here, C denotes the elasticity tensor of the material, and we have abbreviated $A : B = \mathrm{tr}(A^T B)$ for $A, B \in \mathbb{R}^{2\times 2}$. For simplicity we have neglected any body forces. The compliance measures the mechanical work of the load and thus can be interpreted as the inverse structural rigidity.

Fixing a domain of interest $\Omega \subset \mathbb{R}^2$ with $\Gamma \subset \partial\Omega$ one now seeks the geometry $\mathcal{O} \subset \Omega$ which minimizes the compliance under a constraint or a penalty on the volume $\mathrm{Vol}(\mathcal{O}) = \int_{\mathcal{O}} 1\mathrm{d}x$, which may be interpreted as the material weight or material costs. To prevent geometries with infinitely fine microstructure and thereby ensure existence of minimizers (see e. g. [2, 6]), additional regularization is required such as a penalization of the geometry perimeter $\mathrm{Per}(\mathcal{O}) = \mathcal{H}^1(\partial\mathcal{O})$ ($\mathcal{H}^1$ denotes the one-dimensional Hausdorff measure). Note that since we penalize $\mathrm{Per}(\mathcal{O})$ we will always work with geometries of finite perimeter, and throughout this article $\partial\mathcal{O}$ shall refer to the so-called essential boundary of $\mathcal{O}$ [5]. The perimeter regularization may be regarded as a measure of structural complexity or production costs of the design. Altogether we are led to the optimization problem of finding the optimal shape $\mathcal{O} \subset \Omega$ with respect to the objective functional

$$\mathrm{J}[\mathcal{O}] = \alpha\mathrm{Comp}(\mathcal{O}) + \beta\mathrm{Vol}(\mathcal{O}) + \varepsilon\mathrm{Per}(\mathcal{O})$$

for weighting parameters $\alpha, \beta, \varepsilon > 0$.

Compliance minimization represents by now a classical field in optimal design and has been mathematically analyzed and numerically implemented in different

variants, using level set formulations [4], phase field approaches [7, 24, 22], multiple materials [7, 24], design-dependent loads [4, 7], nonlinear elasticity [22], or other regularizations such as constraining the topological genus [8]. Alternative objectives to the compliance such as the L^2-norm of the internal stresses or the expected excess compliance for a probability distribution of loads are much less understood but also possible [1, 14].

1.2 Energy scaling law for uniaxial load geometry

In this article we restrict ourselves to the simple case of a rectangular domain $\Omega = [0,\ell] \times [0,L]$ and a boundary load $\hat{\sigma}n$ imposed on $\partial\Omega$ (n denotes the unit outward normal) which is consistent with a uniform uniaxial stress field $\hat{\sigma} = \left(\begin{smallmatrix} 0 & 0 \\ 0 & F \end{smallmatrix}\right)$. In other words, a normal tension of magnitude F is applied at the top and bottom boundary $\Gamma = [0,\ell] \times \{0, L\} \subset \partial\Omega$ (see Figure 1). Note that this load configuration implies the implicit geometry constraint $\partial\mathcal{O} \supset \Gamma$. Furthermore, for simplicity we shall consider an isotropic material with shear modulus μ and zero Poisson's ratio so that the compliance is finally given by $\mathrm{Comp}^{\mu,F,\ell,L}(\mathcal{O}) = \infty$ if $\partial\mathcal{O} \not\supset \Gamma$ and otherwise

$$\mathrm{Comp}^{\mu,F,\ell,L}(\mathcal{O}) = \frac{1}{2}\int_{\partial\Omega} (\hat{\sigma}n)\cdot u \,\mathrm{d}a \quad \text{with } \hat{\sigma} = \left(\begin{smallmatrix} 0 & 0 \\ 0 & F \end{smallmatrix}\right),$$

in which the equilibrium displacement u minimizes the free energy

$$\mathrm{E}^{\mu,F,\ell,L}[u] = \int_{\mathcal{O}} \mu|\epsilon(u)|^2 \,\mathrm{d}x - \int_{\partial\Omega} (\hat{\sigma}n)\cdot u \,\mathrm{d}a$$

(the superscripts here refer to the model parameters). As can be readily verified, the objective functional

$$\mathrm{J}^{\alpha,\beta,\varepsilon,\mu,F,\ell,L}[\mathcal{O}] = \alpha\mathrm{Comp}^{\mu,F,\ell,L}(\mathcal{O}) + \beta\mathrm{Vol}(\mathcal{O}) + \varepsilon\mathrm{Per}(\mathcal{O})$$

satisfies the scale invariance

$$\mathrm{J}^{\alpha,\beta,\varepsilon,\mu,F,\ell,L}[L\mathcal{O}] = \beta L^2 \mathrm{J}^{1,1,\frac{\varepsilon}{\beta L},\frac{1}{4},F\sqrt{\frac{\alpha}{4\mu\beta}},\frac{\ell}{L},1}[\mathcal{O}]$$

so that it suffices to consider the case $\alpha = \beta = L = 1$, $\mu = \frac{1}{4}$ which we will assume throughout. We will show that the optimal geometry satisfies the following scaling law.

Theorem 1 (Optimal energy scaling for uniaxial normal load)**.** *Let $\delta = \frac{1}{16}$. In the regime $|F| < 1-\delta$, $\varepsilon < \min(\ell^3|F|, |F|^4)$, there exist $c, C > 0$ with*

$$c\ell|F|^{\frac{1}{3}}\varepsilon^{\frac{2}{3}} \le \min_{\mathcal{O}\subset\Omega} \mathrm{J}^{\varepsilon,F,\ell}[\mathcal{O}] - \mathrm{J}_0^{*,F,\ell} \le C\ell|F|^{\frac{1}{3}}\varepsilon^{\frac{2}{3}}$$

for $\mathrm{J}_0^{*,F,\ell} = 2\ell|F|$.

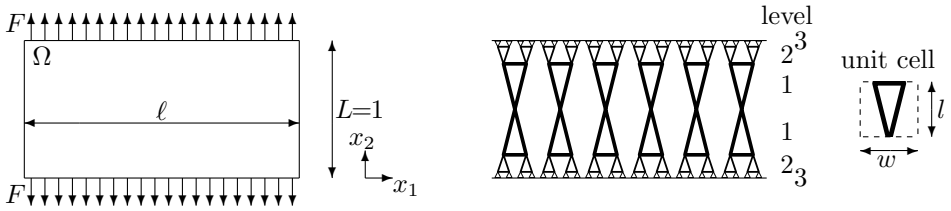

Figure 1: Left: Load geometry considered in this article with a uniform normal tension F at the top and bottom. The optimal design $\mathcal{O}$ is sought inside Ω. Right: Sketch of optimal construction (here with three branching levels), which is composed of several unit cells.

In the above we require $|F|$ to stay bounded away from 1 by some δ, where the choice $\delta = \frac{1}{16}$ just reduces the level of technicality in the proof of the upper inequality. For $|F|$ close to 1, results for related problems (cf. [9, 10] and the later discussion in Section 1.4) suggest a different energy scaling involving a power of $(1-|F|)$. In that case one requires additional constraints on the smallness of ε relative to $(1-|F|)$. Let us also remark that the factor $|F|^{\frac{1}{3}}$ in the scaling law is only relevant for $|F|$ near zero, since it is of order 1 otherwise.

The upper bound is proved in Section 2.1 by constructing a family of designs with the claimed scaling. Those designs follow a classical branching pattern with slight adaptations to compliance optimization (cf. Figure 1). Section 2.2 will then put forward two proofs of how the lower bound scales in ε, one based on convex duality and the other based on a Fourier argument. Alternative proofs of lower bounds are of interest, because they enrich our collection of methods for the analysis of material microstructure. Furthermore, the convex duality proof (in the provided, very elementary and intuitive version) only holds for $|F|$ smaller than and bounded away from $\frac{1}{2}$, in which case it yields the optimal prefactor $c\ell|F|^{\frac{1}{3}}$, while the Fourier argument seems more generalizable but only provides the optimal prefactor for $|F|$ bounded away from 0 and 1.

In the limit $\varepsilon = 0$, minimizing geometries cease to exist since the functional $\mathrm{J}^{0,F,\ell}$ is not lower semi-continuous along sequences of geometries with weakly converging characteristic functions. However, the infimum of $\mathrm{J}^{0,F,\ell}$ can be expressed as the minimum of the relaxation $\mathrm{rel}(\mathrm{J}^{0,F,\ell})$ (the lower semi-continuous envelope), which is given by $\mathrm{J}_0^{*,F,\ell}$ and is well-understood (cf. Section 2 and [19, 20, 21]). In the case of our uniaxial load, the minimizers of the relaxed problem are known to be rank-1 laminates, i. e. near-optimal geometries are almost one-dimensional and consist of very many very thin parallel strands along the loading direction. This is the borderline case between two very different situations:

- In one situation the boundary load is consistent with a uniform stress field $\hat{\sigma}$ with two eigenvalues of opposite sign (e. g. a shear load). In that case the only optimal geometries are known to be rank-2 laminates aligned with the two orthogonal principal stress directions [3]. A one-dimensional

branching as in Section 2.1 then no longer suffices for nonzero ε, and the energy scaling law is quite different [17].

- In the other situation $\hat{\sigma}$ has two eigenvalues of equal sign (e. g. a hydrostatic pressure load). In that case there are many different optimal microstructures such as rank-2 and higher-rank laminates or confocal ellipse constructions. Depending on the shape of Ω there might even be minimizers of $\mathrm{J}^{0,F,\ell}$ without microstructure so that $\min_{\mathcal{O}\subset\Omega} \mathrm{J}^{\varepsilon,F,\ell}[\mathcal{O}]$ is independent of ε: a simple example is the unit disk $\Omega = \{x \in \mathbb{R}^2 \,|\, |x| < 1\}$ under hydrostatic pressure—the optimal geometry $\mathcal{O}$ will be an annulus.

The uniaxial load case treated here is relatively simple and thus serves as a good starting point for the understanding of compliance minimization. Let us finally mention that our restriction to zero Poisson's ratio considerably simplifies the analysis, but is not expected to have a strong influence, since the optimal geometries are composed of truss-like structures for which the lateral contraction is irrelevant.

1.3 Dual reformulation via stress field

It is a classical result in linearized elasticity that the compliance can alternatively be expressed in terms of the equilibrium stress σ instead of the equilibrium displacement u [23]. For our choice of parameters we have

$$\mathrm{Comp}^{F,\ell}(\mathcal{O}) = \int_{\mathcal{O}} |\sigma|^2 \,\mathrm{d}x = \min_{\tilde{\sigma}\in\Sigma^{\mathcal{O}}_{\mathrm{ad}}} \int_{\mathcal{O}} |\tilde{\sigma}|^2 \,\mathrm{d}x\,,$$

where the set $\Sigma^{\mathcal{O}}_{\mathrm{ad}}$ of statically admissible stress fields is given by divergence-free symmetric tensor fields satisfying the prescribed stress boundary conditions,

$$\Sigma^{\mathcal{O}}_{\mathrm{ad}} = \{\sigma : \Omega \to \mathbb{R}^{2\times 2}_{\mathrm{sym}} \,|\, \mathrm{div}\sigma = 0 \text{ in } \Omega, \sigma = 0 \text{ in } \Omega\setminus\mathcal{O}, \sigma n = \hat{\sigma} n \text{ on } \partial\Omega\}\,.$$

Indeed, testing the Euler–Lagrange equation for the equilibrium displacement, $\partial_u \mathrm{E}^{F,\ell}[u] = 0$, with u itself, we obtain

$$\mathrm{Comp}^{F,\ell}(\mathcal{O}) = \frac{1}{2}\int_{\partial\Omega} (\hat{\sigma} n)\cdot u \,\mathrm{d}a = \int_{\mathcal{O}} \frac{1}{4}|\epsilon(u)|^2 \,\mathrm{d}x = -\mathrm{E}^{F,\ell}[u]\,.$$

Furthermore, by Fenchel duality,

$$\int_{\mathcal{O}} \frac{1}{4}|\epsilon(\tilde{u})|^2 + |\tilde{\sigma}|^2 \,\mathrm{d}x \geq \int_{\mathcal{O}} \tilde{\sigma} : \epsilon(\tilde{u}) \,\mathrm{d}x = \int_{\partial\mathcal{O}} (\tilde{\sigma} n)\cdot \tilde{u} \,\mathrm{d}a - \int_{\mathcal{O}} \mathrm{div}\tilde{\sigma}\cdot\tilde{u}\,\mathrm{d}x$$

with equality if and only if $\tilde{\sigma} = \frac{1}{2}\epsilon(\tilde{u})$, i. e. $\tilde{\sigma}$ is the stress induced by the displacement $\tilde{u}$. Hence, for any $\tilde{u}$ and $\tilde{\sigma} \in \Sigma^{\mathcal{O}}_{\mathrm{ad}}$ we have

$$\int_{\mathcal{O}} |\tilde{\sigma}|^2 \,\mathrm{d}x \geq \int_{\partial\Omega} (\tilde{\sigma} n)\cdot\tilde{u}\,\mathrm{d}a - \int_{\mathcal{O}} \frac{1}{4}|\epsilon(\tilde{u})|^2 \,\mathrm{d}x = -\mathrm{E}^{F,\ell}[\tilde{u}]\,,$$

which implies the desired expression for the compliance. Summarizing, an alternative formulation of the compliance minimization problem reads

$$\min_{\mathcal{O}\subset\Omega} \mathrm{J}^{\varepsilon,F,\ell}[\mathcal{O}] \quad \text{for } \mathrm{J}^{\varepsilon,F,\ell}[\mathcal{O}] = \min_{\tilde{\sigma}\in\Sigma_{\mathrm{ad}}^{\mathcal{O}}} \int_{\mathcal{O}} |\tilde{\sigma}|^2 \,\mathrm{d}x + \mathrm{Vol}(\mathcal{O}) + \varepsilon \mathrm{Per}(\mathcal{O}) \,.$$

1.4 Two related optimal design problems

Compliance minimization can be viewed as PDE-constrained optimization in which the PDE constraint is vector-valued. The corresponding scalar version is the optimization of a heat or electricity conductor for prescribed normal flux $\hat{f}\cdot n : \partial\Omega \to \mathbb{R}$ with $\hat{f} = \left(\begin{smallmatrix} 0 \\ F \end{smallmatrix}\right)$ on the boundary, i. e.

$$\text{minimize } \mathrm{J}_{\mathrm{scal}}^{\varepsilon,F,\ell}[\mathcal{O}] = \mathrm{Diss}^{F,\ell}(\mathcal{O}) + \mathrm{Vol}(\mathcal{O}) + \varepsilon \mathrm{Per}(\mathcal{O}) \,,$$

where the energy dissipation is defined as

$$\mathrm{Diss}^{F,\ell}(\mathcal{O}) = \frac{1}{2}\int_{\partial\Omega} (\hat{f}\cdot n) u \,\mathrm{d}x \quad \text{for } u = \operatorname*{argmin}_{\tilde{u}:\mathcal{O}\to\mathbb{R}} \int_{\mathcal{O}} \frac{1}{4}|\nabla\tilde{u}|^2 \,\mathrm{d}x - \int_{\partial\Omega} (\hat{f}\cdot n)\tilde{u} \,\mathrm{d}x$$

with $u : \mathcal{O} \to \mathbb{R}$ the equilibrium temperature or electric potential. The corresponding dual reformulation via fluxes $f = \nabla u$ reads

$$\min_{\mathcal{O}\subset\Omega} \mathrm{J}_{\mathrm{scal}}^{\varepsilon,F,\ell}[\mathcal{O}] \quad \text{for } \mathrm{J}_{\mathrm{scal}}^{\varepsilon,F,\ell}[\mathcal{O}] = \min_{\tilde{f}\in\Phi_{\mathrm{ad}}^{\mathcal{O}}} \int_{\mathcal{O}} |\tilde{f}|^2 \,\mathrm{d}x + \mathrm{Vol}(\mathcal{O}) + \varepsilon \mathrm{Per}(\mathcal{O}) \,,$$

where the set of admissible fluxes is given by

$$\Phi_{\mathrm{ad}}^{\mathcal{O}} = \{f : \Omega \to \mathbb{R}^2 \,|\, \mathrm{div} f = 0 \text{ in } \mathcal{O}, f = 0 \text{ in } \Omega\setminus\mathcal{O}, f\cdot n = \hat{f}\cdot n \text{ on } \partial\Omega\} \,.$$

In the above scalar problem, a pointwise flux constraint $\nabla u\cdot n = f\cdot n = \hat{f}\cdot n$ on $\partial\Omega$ is imposed. A less restrictive problem formulation is to extend the flux to $\mathbb{R}^2$ and just penalize the difference $f - \hat{f}$ on $\mathbb{R}^2\setminus\Omega$,

$$\min_{\mathcal{O}\subset\Omega} \mathrm{J}_{\mathrm{scal,rel}}^{\varepsilon,F,\ell}[\mathcal{O}] \quad \text{for } \mathrm{J}_{\mathrm{scal,rel}}^{\varepsilon,F,\ell}[\mathcal{O}] = \min_{\tilde{f}\in\Phi_{\mathrm{ad,rel}}^{\mathcal{O}}} \int_{\mathcal{O}} |\tilde{f}|^2 \,\mathrm{d}x + \int_{\mathbb{R}^2\setminus\Omega} |\tilde{f}-\hat{f}|^2 \,\mathrm{d}x + \mathrm{Vol}(\mathcal{O}) + \varepsilon \mathrm{Per}(\mathcal{O})$$

with

$$\Phi_{\mathrm{ad,rel}}^{\mathcal{O}} = \{f : \mathbb{R}^2 \to \mathbb{R}^2 \,|\, \mathrm{div} f = 0 \text{ in } \mathbb{R}^2, f = 0 \text{ on } \Omega\setminus\mathcal{O}\} \,.$$

This can also be interpreted as penalizing the $H^{-\frac{1}{2}}$-norm of $f - \hat{f}$ on $\partial\Omega$ instead of strictly requiring $f\cdot n = \hat{f}\cdot n$ on $\partial\Omega$ [12]. This latter optimization problem turns out to be equivalent to the variational pattern formation problem in intermediate states of type-I superconductors: If an external magnetic field $\hat{f} = \left(\begin{smallmatrix} 0 \\ F \end{smallmatrix}\right)$ is applied to a sample $\Omega \subset \mathbb{R}^2$ of superconducting material, then the material spontaneously partitions into superconducting and normal regions, and an induced magnetic field $f : \mathbb{R}^2 \to \mathbb{R}^2$ develops, which is divergence-free and zero in the superconducting region. Denoting by $\mathcal{O}$ the normal region, the free energy

can be modeled as being composed of a magnetic term and a small interfacial energy between both regions [9],

$$\mathrm{J}_{\mathrm{SC}}^{\varepsilon,F,\ell}[\mathcal{O}] = \min_{f\in\Phi_{\mathrm{ad,rel}}^{\mathcal{O}}} \int_{\mathcal{O}\cup(\mathbb{R}^2\setminus\Omega)} |f-\hat{f}|^2 \,\mathrm{d}x + \int_{\Omega\setminus\mathcal{O}} |\hat{f}|^2 - 1 \,\mathrm{d}x + \varepsilon\mathrm{Per}(\mathcal{O})\,.$$

The relaxed energy for $\varepsilon = 0$ has the minimum $\mathrm{J}_{\mathrm{SC},0}^{*,F,\ell} = -(|F|-1)^2\ell$. Using $\int_0^\ell f_2(x_1,x_2)\,\mathrm{d}x_1 = F\ell$ for any $f \in \Phi_{\mathrm{ad,rel}}^{\mathcal{O}}$ and every cross-section x_2, we obtain

$$\begin{aligned}\mathrm{J}_{\mathrm{SC}}^{\varepsilon,F,\ell}[\mathcal{O}] - \mathrm{J}_{\mathrm{SC},0}^{*,F,\ell} = \min_{f\in\Phi_{\mathrm{ad,rel}}^{\mathcal{O}}} &\int_{\mathcal{O}} |f|^2 - 2f\cdot\hat{f}\,\mathrm{d}x + \int_{\Omega} |\hat{f}|^2 - 1\,\mathrm{d}x + \int_{\mathbb{R}^2\setminus\Omega} |f-\hat{f}|^2\,\mathrm{d}x \\ &+ \mathrm{Vol}(\mathcal{O}) + \varepsilon\mathrm{Per}(\mathcal{O}) + (|F|-1)^2\ell = \mathrm{J}_{\mathrm{scal,rel}}^{\varepsilon,F,\ell}[\mathcal{O}] - \mathrm{J}_0^{*,F,\ell}\,.\end{aligned}$$

By a straightforward adaptation of the proofs presented in the next section, the energy scaling Theorem 1 is also valid for the above presented scalar and relaxed scalar problem. In fact, by choosing the second row of $\tilde{\sigma} : \Omega \to \mathbb{R}^{2\times 2}_{\mathrm{sym}}$ as a test flux $\tilde{f} : \Omega \to \mathbb{R}^2$, we find

$$\mathrm{J}^{\varepsilon,F,\ell}[\mathcal{O}] \geq \mathrm{J}_{\mathrm{scal}}^{\varepsilon,F,\ell}[\mathcal{O}] \geq \mathrm{J}_{\mathrm{scal,rel}}^{\varepsilon,F,\ell}[\mathcal{O}]$$

so that the upper bound would only have to be proven for the compliance minimization and the lower bound for the type-I superconductor problem. Nevertheless, in the next section we shall present the proof of the upper as well as the lower bound in the context of compliance minimization, since the convex duality proof of the lower bound is very instructive and intuitive, and the Fourier-type argument for the lower bound will form the basis for the analysis of a compliance minimization scaling law in the more complicated case of an imposed shear load.

Note that the scaling law of the type-I superconductor problem has already been proven in [9] (improved estimates for extreme regimes of small or large applied field in 3D are given in [10]). The lower bound is obtained by simply observing that the energy is larger than the energy of a particular micromagnetic pattern formation problem with known energy scaling law. This micromagnetic scaling law was derived in 2D in [11], following the classic approach due to Kohn and Müller [18] which we also present for compliance minimization in Section 2.2.1, and in 3D in [12], where the argument is based on interpolation inequalities whose derivation is not unlike the Fourier-based proof of the lower bound presented in Section 2.2.2.

2 Energy scaling of optimal elastic design for uniaxial load

In this section we prove the energy scaling law Theorem 1 for the load case from Figure 1 and the compliance minimization energy

$$\mathrm{J}^{\varepsilon,F,\ell}[\mathcal{O}] = \min_{\sigma\in\Sigma_{\mathrm{ad}}^{\mathcal{O}}} \int_{\mathcal{O}} |\sigma|^2\,\mathrm{d}x + \mathrm{Vol}(\mathcal{O}) + \varepsilon\mathrm{Per}(\mathcal{O})\,.$$

As previously discussed, for nonzero ε one pays an excess energy over $\mathrm{J}_0^{*,F,\ell} = \inf_{\mathcal{O}\subset\Omega} \mathrm{J}^{0,F,\ell}[\mathcal{O}]$. By identifying $\mathcal{O}$ with all those points in Ω where the stress field is nonzero, we can express this infimum as

$$\mathrm{J}_0^{*,F,\ell} = \inf_{\sigma\in\Sigma^\Omega_{\mathrm{ad}}} \int_\Omega g(\sigma)\,\mathrm{d}x \quad \text{with } g(\sigma) = \begin{cases} 0 & \text{if } \sigma = 0\,, \\ |\sigma|^2 + 1 & \text{else.} \end{cases}$$

The integral is not lower semi-continuous with respect to a weakly converging sequence of stress fields σ so that the infimum is not achieved, however, one may replace the infimum by the minimum of the lower semi-continuous envelope, which is obtained by quasi-convexifying the integrand g and which in [19, 20, 21] is shown to be

$$\mathrm{J}_0^{*,F,\ell} = \min_{\sigma\in\Sigma^\Omega_{\mathrm{ad}}} \int_\Omega \tilde{g}(\sigma)\,\mathrm{d}x \quad \text{with } \tilde{g}(\sigma) = \begin{cases} 2(|\sigma_1| + |\sigma_2| - |\sigma_1\sigma_2|) & \text{if } |\sigma_1| + |\sigma_2| \le 1, \\ 1 + \sigma_1^2 + \sigma_2^2 & \text{else.} \end{cases}$$

The minimum value $\mathrm{J}_0^{*,F,\ell} = 2\ell|F|$ for $|F| \le 1$ is achieved by $\sigma = \hat{\sigma}$.

Intuitively, due to the uniaxial load geometry only one row of the stress field σ contributes to the relaxed energy. For integrands with vector-valued arguments, quasi-convexification is equivalent to convexification, and indeed we also have $\mathrm{J}_0^{*,F,\ell} = \min_{\sigma\in\Sigma^\Omega_{\mathrm{ad}}} \int_\Omega g^{**}(\sigma)\,\mathrm{d}x$ for the convexification g^{**} of g with $g^{**}(\sigma) = 2|\sigma|$ if $|\sigma| < 1$ and $g^{**}(\sigma) = 1 + |\sigma|^2$ else. This gives a hint as to why convex duality techniques suffice for the proof of a lower bound in Section 2.2.1.

We will next prove the upper bound and then provide two different arguments for the lower bound. In the following, for two expressions A and B we shall abbreviate by $A \lesssim B$ that there exists an independent constant C for which $A \le CB$. $A \gtrsim B$ will be used equivalently to $B \lesssim A$, and $A \sim B$ shall stand for $A \lesssim B$ and $B \lesssim A$.

2.1 Upper bound: A classical branching construction

Close to the center $x_2 \sim \frac{1}{2}$, near-optimal structures must be very coarse to save interfacial energy, while the material must be distributed quite evenly along the boundary $x_2 \sim 0, x_2 \sim 1$ in order to support the load. Hence one may expect a stepwise structural refinement from the center to the boundary via branching (cf. Figure 1), similar to constructions known from type-I superconductors [9]. As is most useful for branching constructions, we shall proceed in the standard steps; also we just consider the upper half $x_2 \in [\frac{1}{2}, 1]$ for the construction since the lower one will be symmetric.

Step 1. Specify the geometry of a unit cell and find its excess energy and optimal aspect ratio. The typical tree-like branching structure from type-I superconductors or similar problems (Figure 2) does not suffice since all branches will bend towards each other under load, producing lots of compliance. However, by introducing a cross-truss in between all branching pairs, the tree

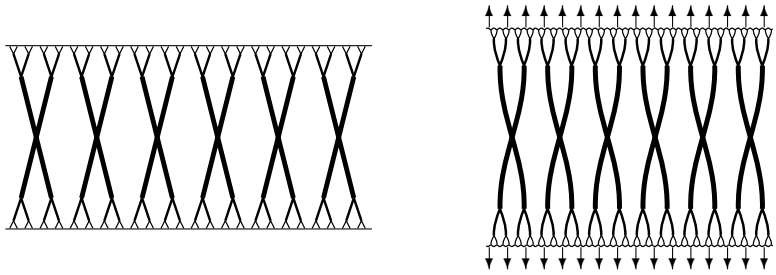

Figure 2: Left: Classical branching structure describing the pattern emerging in intermediate states of type-I superconductors. Right: Deformation of the same structure under a tension load. All branches bend, which results in a high compliance.

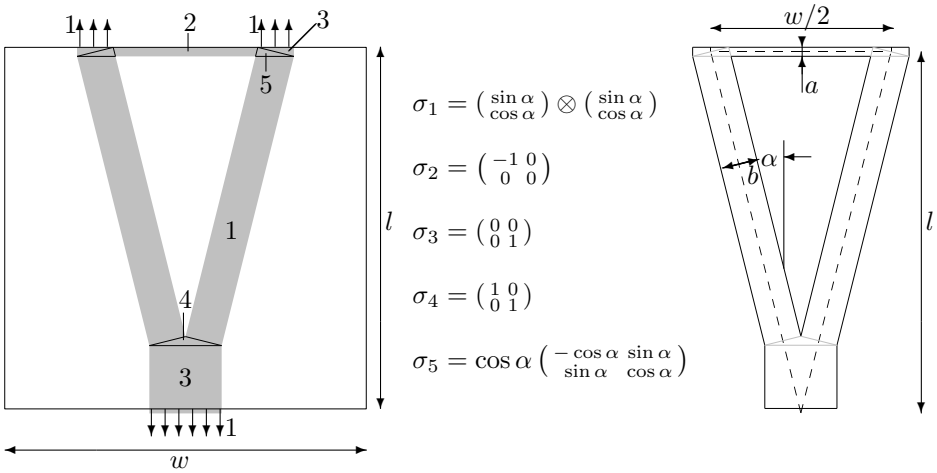

Figure 3: Sketch of a unit cell; the domains of constant stress are numbered. The right graph serves to indicate the geometric parameters.

turns into a truss structure in which each truss is either compressed or dilated, which costs much less than bending.

The unit cell of width w and height l is depicted in Figure 3. The total normal load acting on its top or bottom is given by $|F|w$. In order to have uniaxial stress of magnitude 1 in each truss (which from the convexification of g we know to be a preferred value) we choose $a = \frac{|F|w}{2}\tan\alpha$ and $b = \frac{|F|w}{2\cos\alpha}$, where $\tan\alpha = w/4l$ and we will ensure $w/l \le 1$. The excess energy over the relaxed energy $2|F|wl$ per unit cell for $\varepsilon = 0$ can then be estimated as

$$\Delta \mathrm{J}_{\mathrm{cell}} = \mathrm{Comp}_{\mathrm{cell}} + \mathrm{Vol}_{\mathrm{cell}} + \varepsilon \mathrm{Per}_{\mathrm{cell}} - 2|F|wl \sim 2(2\tfrac{l}{\cos\alpha}b + a\tfrac{w}{2}) + 4\varepsilon\tfrac{l}{\cos\alpha} + 2\varepsilon\tfrac{w}{2} - 2|F|wl$$
$$\sim 2|F|\tfrac{w}{l}(\tfrac{w^2}{16} + l^2) + |F|\tfrac{w^3}{8l} + 4\varepsilon\sqrt{l^2 + \tfrac{w^2}{16}} + \varepsilon w - 2|F|wl \sim |F|\tfrac{w^3}{l} + \varepsilon(l + w)\,,$$

which is minimized by $l = \sqrt{|F|w^3/\varepsilon}$. We thus choose the dimensions from Figure 3 as

$$l = \sqrt{\tfrac{|F|w^3}{\varepsilon}}\,, \quad \alpha = \arctan(\tfrac{1}{4}\sqrt{\tfrac{\varepsilon}{|F|w}})\,, \quad a = \tfrac{1}{8}\sqrt{|F|w\epsilon}\,, \quad b = \tfrac{|F|w}{2}\sqrt{1 + \tfrac{\varepsilon}{16|F|w}}\,.$$

Using the stress field given in Figure 3, a detailed but straightforward calculation of the total excess energy of the unit cell reveals

$$\Delta \mathrm{J}_{\mathrm{cell}}(w) \lesssim \sqrt{|F|w^3\varepsilon}$$

under the condition $w < l$.

Step 2. Compute coarsest unit cell width and estimate total bulk energy. At $x_2 = \frac{1}{2}$ the width w_{coarse} of the unit cells will be largest, and it will be halved with each new layer of unit cells, i. e. the k^{th} layer has unit cell width $w_k = w_{\mathrm{coarse}}/2^k$ and height $l_k = \sqrt{|F|w_k^3/\varepsilon} = 2^{-3k/2}\sqrt{|F|w_{\mathrm{coarse}}^3/\varepsilon}$. The total height of Ω equals the accumulated height of the unit cell layers. Hence, using n layers,

$$1 = 2\sum_{k=0}^{n} l_k = 2\sqrt{\tfrac{|F|w_{\mathrm{coarse}}^3}{\varepsilon}}\sum_{k=0}^{n} 2^{-\frac{3k}{2}} \sim \sqrt{\tfrac{|F|w_{\mathrm{coarse}}^3}{\varepsilon}}\,,$$

which implies

$$w_{\mathrm{coarse}} \sim \sqrt[3]{\tfrac{\varepsilon}{|F|}}\,.$$

The width of the coarsest unit cell has to be smaller than the width ℓ of Ω from which we obtain the construction constraint

$$\varepsilon \lesssim \ell^3|F|\,.$$

The total bulk excess energy can now be estimated from above by

$$\Delta \mathrm{J}_{\mathrm{bulk}} \le \sum_{i=0}^{n} \tfrac{\ell}{w_i}\Delta \mathrm{J}_{\mathrm{cell}}(w_i) \sim \tfrac{\ell}{w_{\mathrm{coarse}}}\Delta \mathrm{J}_{\mathrm{cell}}(w_{\mathrm{coarse}}) \sim \ell|F|^{\frac{1}{3}}\varepsilon^{\frac{2}{3}}\,.$$

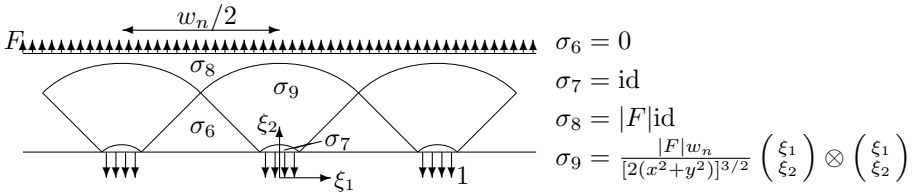

Figure 4: Boundary layer at $x_2 = 1$ with test stress field.

Step 3. Introduce boundary layer. We have to stop layering unit cells as soon as w_k reaches the same size as l_k. This implies the maximum number of layers $n = \log_2(|F|w_{\mathrm{coarse}}/\varepsilon) \sim \frac{2}{3}\log_2(|F|/\varepsilon)$ from which we obtain the constraint $\varepsilon \lesssim |F|$ for our construction. Furthermore, we have to introduce a boundary layer between this n^{th} layer and $x_2 = 1$. The boundary layer and a corresponding test stress field are shown in Figure 4. Note that $w_n \sim \frac{\varepsilon}{|F|}$ so that the volume of the boundary layer scales like $\ell w_n \sim \frac{\ell\varepsilon}{|F|}$, which is less than $\ell|F|^{\frac{1}{3}}\varepsilon^{\frac{2}{3}}$ as long as

$$\varepsilon \leq |F|^4 .$$

The contribution to the compliance is of the same order. Finally, the perimeter contribution is of order $\ell\varepsilon$, which is even smaller so that altogether the boundary layer does not interfere with the bulk energy scaling.

2.2 Lower bound: A real space and a Fourier approach

We will now prove the inequality

$$c_F \ell \varepsilon^{\frac{2}{3}} \leq \min_{\mathcal{O}\subset\Omega} \mathrm{J}^{\varepsilon,F,\ell}[\mathcal{O}] - \mathrm{J}_0^{*,F,\ell} ,$$

where the constant c_F scales like $|F|^{\frac{1}{3}}$ for $|F|$ close to zero and is of order 1 for $|F|$ bounded away from zero. The first proof imitates the classical approach due to Kohn and Müller [18] and provides a very intuitive idea of how the deformation of near-optimal structures will be distributed. To avoid technicalities, the proof assumes that $|F|$ is smaller than and bounded away from $\frac{1}{2}$. The second approach to prove the lower bound is based on a refinement of the Hashin–Shtrikman bounds for the effective elastic moduli of composite materials. This proof attains the correct scaling in ε, but not quite the correct expression in $|F|$ for the prefactor in the case that $|F|$ is small. Nevertheless we present this proof since it is valid also for $|F| \geq \frac{1}{2}$ and furthermore forms the basis for the analysis of compliance minimization under shear loads [17]. It is an open question whether its deficiency of the suboptimal scaling in $|F|$ can be remedied by a refinement of the argument.

2.2.1 Lower bound by convex duality

Abbreviate $\min_{\mathcal{O}} \mathrm{J}^{F,\varepsilon,\ell}[\mathcal{O}]$ by $\hat{\mathrm{J}}$ and set $\Delta\mathrm{J} = \hat{\mathrm{J}} - \mathrm{J}_0^{F,*,\ell} = \hat{\mathrm{J}} - 2|F|\ell$. From $\Delta\mathrm{J} \geq \varepsilon\mathrm{Per}(\mathcal{O})$ for the optimal $\mathcal{O}$ we obtain that there is a generic cross-section

$x_2 = \hat{x}_2 \sim \frac{1}{2}$ on which (up to a constant factor) there are at most $\frac{\Delta \mathrm{J}}{\varepsilon}$ interfaces. Furthermore, $\hat{\mathrm{J}} \geq \mathrm{Vol}(\mathcal{O})$ implies that the material volume fraction on $\hat{x}_2$ may be assumed to be less than a constant times $\frac{\hat{\mathrm{J}}}{\ell}$, which by the previous section is $\lesssim |F|$. We shall try to compute the excess energy of such a configuration over the relaxed energy $\mathrm{J}_0^{F,*,\ell}$. Assume there are N material gaps on $x_2 = \hat{x}_2$, their union denoted by $\tilde{\Gamma} = ((a_1, b_1) \cup \ldots \cup (a_N, b_N)) \times \{\hat{x}_2\}$. Then

$$\mathrm{J}^{F,\varepsilon,\ell}[\mathcal{O}] = \min_{\substack{\sigma \in \Sigma_{\mathrm{ad}}^{\mathcal{O}} \\ \sigma n = 0 \text{ on } \tilde{\Gamma}}} \int_{\mathcal{O}} |\sigma|^2 \,\mathrm{d}x + \mathrm{Vol}(\mathcal{O}) + \varepsilon \mathrm{Per}(\mathcal{O}) \geq \min_{\substack{\sigma \in \Sigma_{\mathrm{ad}}^{\Omega} \\ \sigma n = 0 \text{ on } \tilde{\Gamma}}} \int_{\Omega} g(\sigma) \,\mathrm{d}x$$

which by convexification is greater than or equal to

$$\begin{aligned}
\min_{\substack{\sigma \in \Sigma_{\mathrm{ad}}^{\Omega} \\ \sigma n = 0 \text{ on } \tilde{\Gamma}}} \int_{\Omega} g^{**}(\sigma) \,\mathrm{d}x &= \min_{\substack{\sigma : \Omega \to \mathbb{R}^{2\times 2}_{\mathrm{sym}} \\ \sigma n = \hat{\sigma} n \text{ on } \partial\Omega \\ \sigma n = 0 \text{ on } \tilde{\Gamma}}} \sup_{u : \Omega \to \mathbb{R}^2} \int_{\Omega} g^{**}(\sigma) + u \cdot \mathrm{div} \sigma \,\mathrm{d}x \\
&= \min_{\sigma : \Omega \to \mathbb{R}^{2\times 2}_{\mathrm{sym}}} \sup_{u : \Omega \to \mathbb{R}^2} \int_{\Omega \setminus \tilde{\Gamma}} g^{**}(\sigma) - \epsilon(u) : \sigma \,\mathrm{d}x + \int_{\partial\Omega} (\hat{\sigma} n) \cdot u \,\mathrm{d}a \\
&\geq \sup_{u : \Omega \to \mathbb{R}^2} \int_{\Omega \setminus \tilde{\Gamma}} \min_{\sigma \in \mathbb{R}^{2\times 2}_{\mathrm{sym}}} g^{**}(\sigma) - \epsilon(u) : \sigma \,\mathrm{d}x + \int_{\partial\Omega} (\hat{\sigma} n) \cdot u \,\mathrm{d}a \\
&= \sup_{u : \Omega \to \mathbb{R}^2} \int_{\Omega \setminus \tilde{\Gamma}} -g^*(\epsilon(u)) \,\mathrm{d}x + \int_{\partial\Omega} (\hat{\sigma} n) \cdot u \,\mathrm{d}a \,,
\end{aligned}$$

where the Lagrange multiplier $u \in H^1(\Omega; \mathbb{R}^2)$ has the interpretation of a displacement and the Legendre–Fenchel dual g^* to g is given by

$$g^*(\epsilon) = (g^{**})^*(\epsilon) = \begin{cases} 0 & \text{if } |\epsilon| \leq 2, \\ \frac{|\epsilon|^2}{4} - 1 & \text{else.} \end{cases}$$

Summarizing, the excess energy $\Delta \mathrm{J}$ is bounded below by

$$\sup_{\substack{u : \Omega \to \mathbb{R}^2 \\ |\epsilon(u)| \leq 2 \text{ on } \Omega \setminus \tilde{\Gamma}}} \int_{\partial\Omega} (\hat{\sigma} n) \cdot u \,\mathrm{d}a - 2|F|\ell \,.$$

We now construct an appropriate test displacement u. Without loss of generality assume the case of $\hat{\sigma}$ being a tension load (for $\hat{\sigma}$ a compression the direction of the displacement is just reversed). The test displacement u is chosen to pull the fissures $\tilde{\Gamma}$ open (cf. Figure 5): Take the ansatz

$$u = \begin{pmatrix} 0 \\ 2\eta x_2 \end{pmatrix} + 2f(x_1) \begin{pmatrix} 0 \\ \mathrm{sgn}(x_2 - \hat{x}_2) \end{pmatrix} \,,\; Du = \begin{pmatrix} 0 & 0 \\ \pm 2f'(x_1) & 2\eta \end{pmatrix} \,,\; \epsilon(u) = \begin{pmatrix} 0 & \pm f'(x_1) \\ \pm f'(x_1) & 2\eta \end{pmatrix}$$

for some $\eta \in \mathbb{R}$ and $f : \mathbb{R} \to \mathbb{R}$ so that $|\epsilon(u)|^2 = 4\eta^2 + 2f'(x_1)^2$. We choose

$$f(x) = \sqrt{2(1 - \eta^2)} \begin{cases} x - a_i & \text{if } x \in [a_i, \frac{a_i + b_i}{2}], \\ b_i - x & \text{if } x \in [\frac{a_i + b_i}{2}, b_i], \\ 0 & \text{else.} \end{cases}$$

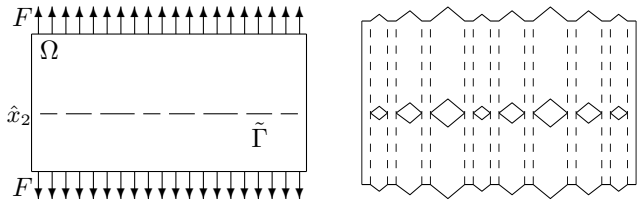

Figure 5: Illustration of the domain Ω with the material gaps $\tilde{\Gamma}$ and of the test displacement, a uniform vertical dilation by the factor $2(1+\eta)$ superimposed with a piecewise linear deformation pulling the fissures $\tilde{\Gamma}$ open.

Introducing $d_i = b_i - a_i$ and $d = \frac{1}{N}\sum_{i=1}^{N} d_i$, we directly obtain

$$\begin{aligned}\int_{\partial\Omega} (\hat{\sigma}n)\cdot u \,\mathrm{d}a - 2|F|\ell &= 2|F|\left[\ell(\eta-1) + \sqrt{\tfrac{1-\eta^2}{2}}\sum_{i=1}^{N} d_i^2\right] \\ &\geq 2|F|\left[\ell(\eta-1) + \sqrt{\tfrac{1-\eta^2}{2}}Nd^2\right] \geq 2|F|\ell\left(\sqrt{1+\tfrac{(Nd)^4}{2N^2\ell^2}}-1\right),\end{aligned}$$

where the last step comes from minimization over η, yielding $\eta^2 = 1/(1+\frac{(Nd)^4}{2N^2\ell^2})$. Using $Nd \gtrsim (\ell - \hat{\mathrm{J}}) \sim \ell$ (here we exploit that $|F|$ lies well below $\frac{1}{2}$) as well as $N \lesssim \frac{\Delta \mathrm{J}}{\varepsilon} \lesssim \ell|F|^{1/3}\varepsilon^{-1/3}$ (from the previous section) we arrive at the bound

$$\Delta \mathrm{J} \gtrsim 2|F|\ell\left(\sqrt{1+\tfrac{1}{2}\big(\tfrac{\varepsilon}{|F|}\big)^{2/3}}-1\right) \gtrsim \ell|F|^{\frac{1}{3}}\varepsilon^{\frac{2}{3}},$$

where we used that $\varepsilon < |F|$.

2.2.2 Lower bound via refined Hashin–Shtrikman bounds

The lower Hashin–Shtrikman bound [15] provides lower estimates on the elastic moduli of composite materials. In particular, given an applied stress field, the Hashin–Shtrikman bound tells us the least compliance with respect to that stress that a microstructured material with prescribed material fraction can have. A neat derivation in discrete Fourier space is given in [3]. We will refine that calculation for our setting in order to extract

(a) the energy costs associated with a deviation of the material trusses from the vertical direction and

(b) the costs associated with a deviation from the optimal material volume.

These two pieces of information will be combined with

(c) a Fourier-estimate that encodes the strict pointwise boundary condition $\sigma n = \hat{\sigma} n$ for the material stress σ and

(d) a Fourier-estimate of $\mathrm{Per}(\mathcal{O})$

to yield the desired bound.

Let $\chi : \Omega \to \{0,1\}$ be the characteristic function of the optimal geometry $\mathcal{O}$ and $\theta = \frac{1}{\mathrm{Vol}(\Omega)} \int_\Omega \chi(x)\,\mathrm{d}x$ be its volume fraction. Furthermore define $\gamma : \mathbb{R}^2 \to \mathbb{R}$ by $\gamma = \chi - \theta$ on Ω, extended by zero outside Ω. For $k \in \mathbb{R}^2 \setminus \{0\}$ abbreviate $\hat{k} = \frac{k}{|k|}$ and denote the Fourier transform of a function $f : \mathbb{R}^2 \to \mathbb{R}$ by

$$\hat{f}(k) = \int_{\mathbb{R}^2} f(x) e^{-2\pi i k\cdot x}\,\mathrm{d}x$$

(the inverse Fourier transform is given by $\check{g}(x) = \int_{\mathbb{R}^2} g(k) e^{2\pi i k\cdot x}\,\mathrm{d}k$). Finally, let Σ^0_{ad} denote the symmetric divergence-free tensor fields on $\mathbb{R}^2$ vanishing outside Ω,

$$\Sigma^0_{\mathrm{ad}} = \{\eta : \mathbb{R}^2 \to \mathbb{R}^{2\times 2}_{\mathrm{sym}} \,|\, \mathrm{div}\eta = 0 \text{ in } \mathbb{R}^2, \eta = 0 \text{ in } \mathbb{R}^2 \setminus \Omega\}\,.$$

Note that those tensor fields have a zero normal component on $\partial\Omega$, $\eta n = 0$. Repeating and adapting the calculation in [3], the refined Hashin–Shtrikman bound is obtained as follows:

$$\begin{aligned}
&\mathrm{Comp}(\mathcal{O}) + \mathrm{Vol}(\mathcal{O})\\
&= \min_{\substack{\eta\in\Sigma^0_{\mathrm{ad}}\\ (\hat\sigma+\eta)(1-\chi)=0 \text{ on } \Omega}} \int_\Omega |\hat\sigma+\eta|^2 + \chi\,\mathrm{d}x\\
&\geq \limsup_{K\to 0} \min_{\eta\in\Sigma^0_{\mathrm{ad}}} \int_\Omega \chi|\hat\sigma+\eta|^2 + \chi + (1-\chi)K^{-1}|\hat\sigma+\eta|^2\,\mathrm{d}x\\
&= \limsup_{K\to 0} \min_{\eta\in\Sigma^0_{\mathrm{ad}}} \int_\Omega |\hat\sigma+\eta|^2 + \chi + (1-\chi)(K^{-1}-1)|\hat\sigma+\eta|^2\,\mathrm{d}x\\
&= \limsup_{K\to 0} \min_{\eta\in\Sigma^0_{\mathrm{ad}}} \int_\Omega |\hat\sigma+\eta|^2 + \chi + (1-\chi)\max_\tau \left[2(\hat\sigma+\eta):\tau - (K^{-1}-1)^{-1}|\tau|^2\right]\mathrm{d}x\,,
\end{aligned}$$

using Fenchel duality in the last step. Assuming the strain τ to be spatially constant and exploiting $\int_\Omega \eta\,\mathrm{d}x = 0$, the previous expression is greater than or equal to

$$\begin{aligned}
&\min_{\eta\in\Sigma^0_{\mathrm{ad}}} \int_\Omega |\hat\sigma+\eta|^2 + \chi + (1-\chi)2(\hat\sigma+\eta):\tau\,\mathrm{d}x\\
=&\mathrm{Vol}(\Omega)(|\hat\sigma|^2 + 2(1-\theta)\hat\sigma:\tau+\theta) + \min_{\eta\in\Sigma^0_{\mathrm{ad}}} \int_{\mathbb{R}^2} |\eta|^2 - 2\gamma\eta:\tau\,\mathrm{d}x\\
\geq&\ell(|\hat\sigma|^2 + 2(1-\theta)\hat\sigma:\tau+\theta) + \min_{\hat\eta(k)\in\mathbb{R}^{2\times 2}_{\mathrm{sym}} \text{ and } \hat\eta(k)\,k=0 \text{ for all } k\in\mathbb{R}^2} \int_{\mathbb{R}^2} |\hat\eta|^2 - 2\overline{\hat\gamma}\hat\eta:\tau\,\mathrm{d}k
\end{aligned}$$

using Parseval's identity. Letting superscript $\perp$ denote a counter-clockwise rotation by $\frac{\pi}{2}$, this expression is minimized by $\hat\eta = \hat\gamma(\hat{k}^\perp\cdot\tau\hat{k}^\perp)\hat{k}^\perp\otimes\hat{k}^\perp$, yielding

$$\ell(|\hat\sigma|^2 + 2(1-\theta)\hat\sigma:\tau+\theta) - \int_{\mathbb{R}^2} |\hat\gamma|^2|\hat{k}^\perp\cdot\tau\hat{k}^\perp|^2\,\mathrm{d}k$$

$$=\ell(|\hat\sigma|^2+2(1-\theta)\hat\sigma:\tau+\theta-\theta(1-\theta)\max(\tau_1^2,\tau_2^2))+\int_{\mathbb{R}^2}|\hat\gamma|^2[\max(\tau_1^2,\tau_2^2)-|\hat k^\perp\cdot\tau\hat k^\perp|^2]\,\mathrm{d}k\,,$$

using $\int_{\mathbb{R}^2}|\hat\gamma|^2\,\mathrm{d}x=\int_\Omega|\gamma|^2\,\mathrm{d}x=\ell\theta(1-\theta)$. Here, τ_1 and τ_2 denote the two singular values of τ. The integral is non-negative, and the remainder is maximized by $\tau=\frac{\hat\sigma}{\hat\theta}$, which we shall assume from now on. Given this τ, the integrand behaves like $\frac{F^2}{\theta^2}|\hat\gamma|^2\frac{k_2^2}{k_1^2+k_2^2}$ so that altogether the excess compliance and volume are estimated below by

$$\begin{aligned}\Delta\mathrm{J}_{\mathrm{elast}}&=\mathrm{Comp}(\mathcal{O})+\mathrm{Vol}(\mathcal{O})-\mathrm{J}_0^{*,F,\ell}\\&\gtrsim\ell(\tfrac{1}{\theta}F^2+\theta-2|F|)+\tfrac{F^2}{\theta^2}\int_{\mathbb{R}^2}|\hat\gamma|^2\tfrac{k_2^2}{k_1^2+k_2^2}\,\mathrm{d}k\\&=\ell\tfrac{(|F|-\theta)^2}{\theta}+\tfrac{F^2}{\theta^2}\int_{\mathbb{R}^2}|\hat\gamma|^2\tfrac{k_2^2}{k_1^2+k_2^2}\,\mathrm{d}k\,.\end{aligned}$$

This estimate quantifies the penalty for deviating from the material fraction $\theta=|F|$ and for the Fourier coefficients of χ or rather γ lying away from the horizontal axis.

Since from the upper bound we know $\Delta\mathrm{J}_{\mathrm{elast}}\lesssim\ell|F|^{1/3}\varepsilon^{2/3}$, we directly see $|F|^{1/3}\varepsilon^{2/3}\gtrsim\frac{(|F|-\theta)^2}{\theta}=|F|(\frac{|F|}{\theta}-1)(1-\frac{\theta}{|F|})$, which can be solved for $\frac{|F|}{\theta}$ to yield $\frac{|F|}{\theta}=1+O((\varepsilon/|F|)^{1/3})\sim1$. Hence, we may reduce the above estimate to

$$\Delta\mathrm{J}_{\mathrm{elast}}\gtrsim\int_{\mathbb{R}^2}|\hat\gamma|^2\tfrac{k_2^2}{k_1^2+k_2^2}\,\mathrm{d}k\,.$$

The fact that the structure $\mathcal{O}$ stops abruptly at $x_2=0,1$ and has to bear a load there enters via the continuous Fourier space analog of [12, Lemma 2.4], which essentially says that the major L^2-mass of a (characteristic) function with support in Ω lies beyond the k_2-frequency $|k_2|=1$ in Fourier space. For the sake of completeness and readability, let us briefly reproduce the short argument:

$$\begin{aligned}\int_{\mathbb{R}}|\hat\gamma|^2\tfrac{k_2^2}{k_1^2+k_2^2}\,\mathrm{d}k_2&\geq\int_{|k_2|>\frac14}|\hat\gamma|^2\tfrac{k_2^2}{k_1^2+k_2^2}\,\mathrm{d}k_2\\&\geq\tfrac{1}{16k_1^2+1}\left(\int_{\mathbb{R}}|\hat\gamma|^2\,\mathrm{d}k_2-\int_{|k_2|\leq\frac14}|\hat\gamma|^2\,\mathrm{d}k_2\right)\geq\tfrac12\tfrac{1}{16k_1^2+1}\int_{\mathbb{R}}|\hat\gamma|^2\,\mathrm{d}k_2\,,\end{aligned}$$

where in the last step we have used $|\hat f|^2\leq\|f\|^2_{L^2([0,1])}=\|\hat f\|^2_{L^2(\mathbb{R})}$ for any $f:[0,1]\to\mathbb{R}$ by Hölder's inequality so that $\int_{|k_2|\leq\frac14}|\hat\gamma|^2\,\mathrm{d}k_2\leq\frac12\int_{\mathbb{R}}|\hat\gamma|^2\,\mathrm{d}k_2$. By Fubini's theorem we thus arrive at

$$\Delta\mathrm{J}_{\mathrm{elast}}\gtrsim\int_{\mathbb{R}^2}|\hat\gamma|^2\tfrac{1}{1+k_1^2}\,\mathrm{d}k\,.$$

Finally, we estimate the perimeter $\mathrm{Per}(\mathcal{O})$ in Fourier space by a technique analogous to the proof of [16, Lemma 3]:

$$\begin{aligned}\mathrm{Per}(\mathcal{O}) &\gtrsim \frac{1}{L}\int_{L/2}^{2L}\frac{1}{s}\|\gamma-\gamma(\cdot+s,\cdot)\|_{L^2(\mathbb{R}^2)}^2\,\mathrm{d}s \sim \frac{1}{L^2}\int_{L/2}^{2L}\int_{\mathbb{R}^2}|\hat{\gamma}(k)(1-e^{2\pi i s k_1})|^2\,\mathrm{d}k\,\mathrm{d}s\\ &\geq \frac{1}{L^2}\int_{L|k_1|\geq 1}|\hat{\gamma}|^2\int_{L/2}^{2L}|1-e^{2\pi i s k_1}|^2\,\mathrm{d}s\,\mathrm{d}k \gtrsim \frac{1}{L}\int_{L|k_1|\geq 1}|\hat{\gamma}|^2\,\mathrm{d}k\end{aligned}$$

for any (small) length scale $L>0$.

Combining the estimates for $\Delta\mathrm{J}_{\mathrm{elast}}$ and $\mathrm{Per}(\mathcal{O})$ and assuming $L\lesssim 1$,

$$\begin{aligned}&\frac{\Delta\mathrm{J}_{\mathrm{elast}}}{L^2}+L\mathrm{Per}(\mathcal{O}) \sim \Delta\mathrm{J}_{\mathrm{elast}}(1+\tfrac{1}{L^2})+L\mathrm{Per}(\mathcal{O})\\ &\gtrsim (1+\tfrac{1}{L^2})\int_{L|k_1|\leq 1}\tfrac{1}{1+k_1^2}|\hat{\gamma}|^2\,\mathrm{d}k+\int_{L|k_1|\geq 1}|\hat{\gamma}|^2\,\mathrm{d}k \geq \int_{\mathbb{R}^2}|\hat{\gamma}|^2\,\mathrm{d}k=\ell\theta(1-\theta)\,.\end{aligned}$$

The choice $L=\varepsilon^{\frac{1}{3}}$ now yields

$$\Delta\mathrm{J}_{\mathrm{elast}}+\varepsilon\mathrm{Per}(\mathcal{O})\gtrsim \ell\theta(1-\theta)\varepsilon^{\frac{2}{3}}\gtrsim \ell|F|\varepsilon^{\frac{2}{3}}\,.$$

For $|F|$ bounded away from 0, this bound behaves like $\ell\varepsilon^{\frac{2}{3}}$, which was to be shown. For $|F|$ close to zero, however, note that the obtained scaling in $|F|$ is suboptimal.

3 Discussion

Let us here briefly comment on the differences between the structural design task treated here and related problems.

Compared to the geometry optimization problem under a scalar PDE constraint, $\min_{\mathcal{O}\subset\Omega}\mathrm{J}_{\mathrm{scal}}^{\varepsilon,F,\ell}$, the energy scaling is the same (cf. Section 1.4). Furthermore, as explained in Section 1.4, the two rows of a stress field can be interpreted as two decoupled fluxes of a scalar quantity so that any test geometry and associated test stress for $\mathrm{J}^{\varepsilon,F,\ell}$ yield a test geometry and test flux for $\mathrm{J}_{\mathrm{scal}}^{\varepsilon,F,\ell}$. However, the opposite is not true so that both optimization problems are not equivalent. Indeed, a geometry with optimal energy scaling for $\mathrm{J}_{\mathrm{scal}}^{\varepsilon,F,\ell}$ is typically not sufficient for $\mathrm{J}^{\varepsilon,F,\ell}$. The reason lies in the fact that elastic deformations satisfy two balance equations instead of a single one: the conservation of linear momentum, which expresses that the stress field is divergence-free (a condition also present in the scalar problem), as well as the conservation of angular momentum, which can be expressed as a symmetry constraint on the stress and is special to the elasticity setting. The symmetry of the stress tensor implies that its rows are actually not two independent fluxes. Choosing a near-optimal flux for $\mathrm{J}_{\mathrm{scal}}^{\varepsilon,F,\ell}$ as one row of the stress field thus induces a constraint for the other row, which typically produces very unfavorable energy. Mechanically, this additional conservation of angular momentum manifests as energy-costly bending

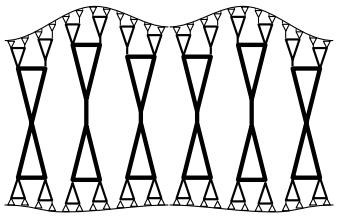

Figure 6: Construction for perturbed load boundaries.

of the geometry (cf. Figure 2). As a remedy, cross-trusses have to be introduced as in Figure 1.

In case of an applied shear load $\hat{\sigma} = \left(\begin{smallmatrix} 0 & F \\ F & 0 \end{smallmatrix}\right)$, the energy scaling is different (for details we refer to [17]). A shear load can be interpreted as a superposition of a uniaxial tension and an orthogonal uniaxial compression. Hence, in a near-optimal geometry we expect to see branching trees similar to the construction from Section 2.1, only in two orthogonal directions. It turns out that the branching trees occur on two different scales: along one direction they extend over the whole domain (just as for the uniaxial load), along the other direction they only connect the different larger branching trees. In [17], the proof of the lower bound is based on a refinement of the Hashin–Shtrikman bounds analogous to Section 2.2.2. The ingredients (a) to (d) are essentially the same, only they have to be adapted and augmented by two further estimates: estimate (a) now has to express the cost associated with a deviation of the geometry from the two preferred orthogonal directions, and the two additional estimates penalize an unbalanced material distribution and an unbalanced spatial distribution between the two directions.

Finally, let us note that slight variations of the load geometry will not alter the energy scaling. For instance, the proofs of lower and upper bound still apply if at $x_1 = 0$ and $x_2 = \ell$ we consider periodic instead of homogeneous Neumann boundary conditions. Also, if the upper and lower boundary are slightly perturbed normally into a smooth but e. g. no longer straight curve, the proof of the lower bound remains valid with the obvious modifications, while the construction has to be adapted a little as indicated in Figure 6: unit cells are shifted up or down and connected to unit cells on the next hierarchy level via vertical struts. As a final note on the corresponding 3D problem, in analogy to the pattern formation in type-I superconductors [10] we expect a richer behavior with a number of different optimal geometries for different regimes. Future work will deal with this and other 3D cases.

References

[1] G. Allaire, F. Jouve, and H. Maillot. Topology optimization for minimum stress design with the homogenization method. *Struct Multidisc Optim*, 28:87–98, 2004.

[2] Grégoire Allaire. *Shape optimization by the homogenization method*, volume 146 of *Applied Mathematical Sciences*. Springer-Verlag, New York, 2002.

[3] Grégoire Allaire and Sylvie Aubry. On optimal microstructures for a plane shape optimization problem. *Structural Optimization*, 17:86–94, 1999.

[4] Grégoire Allaire, Francois Jouve, and Anca-Maria Toader. Structural optimization using sensitivity analysis and a level-set method. *Journal of computational physics*, 194:363–393, 2004.

[5] Luigi Ambrosio, Nicola Fusco, and Diego Pallara. *Functions of bounded variation and free discontinuity problems*. Oxford Mathematical Monographs. Oxford University Press, New York, 2000.

[6] M. P. Bendsøe and O. Sigmund. *Topology optimization: theory, methods and applications*. Springer-Verlag, Berlin, 2003.

[7] B. Bourdin and A. Chambolle. Design-dependent loads in topology optimization. *ESAIM Control Optim. Calc. Var.*, 9:19–48, 2003.

[8] Antonin Chambolle. A density result in two-dimensional linearized elasticity, and applications. *Archive for Rational Mechanics and Analysis*, 167(3):211–233, 2003.

[9] R. Choksi, R. V. Kohn, and F. Otto. Energy minimization and flux domain structure in the intermediate state of a type-I superconductor. *J. Nonlinear Sci.*, 14(2):119–171, 2004.

[10] Rustum Choksi, Sergio Conti, Robert V. Kohn, and Felix Otto. Ground state energy scaling laws during the onset and destruction of the intermediate state in a type I superconductor. *Comm. Pure Appl. Math.*, 61(5):595–626, 2008.

[11] Rustum Choksi and Robert V. Kohn. Bounds on the micromagnetic energy of a uniaxial ferromagnet. *Comm. Pure Appl. Math.*, 51(3):259–289, 1998.

[12] Rustum Choksi, Robert V. Kohn, and Felix Otto. Domain branching in uniaxial ferromagnets: a scaling law for the minimum energy. *Comm. Math. Phys.*, 201(1):61–79, 1999.

[13] P. G. Ciarlet. *Three-dimensional elasticity*. Elsevier Science Publishers B. V., 1988.

[14] Sergio Conti, Harald Held, Martin Pach, Martin Rumpf, and Rüdiger Schultz. Risk averse shape optimization. *SIAM Journal on Control and Optimization*, 49(3):927–947, 2011.

[15] Z. Hashin and S. Shtrikman. A variational approach to the theory of the elastic behaviour of multiphase materials. *J. Mech. Phys. Solids*, 11:127–140, 1963.

[16] Hans Knüpfer, Robert V. Kohn, and Felix Otto. Nucleation barriers for the cubic-to-tetragonal phase transformation. *Comm. Pure Appl. Math.*, 66(6):867–904, 2013.

[17] Robert Kohn and Benedikt Wirth. Optimal microstructures in compliance minimization for a shear load. *in preparation*, 2013.

[18] Robert V. Kohn and Stefan Müller. Surface energy and microstructure in coherent phase transitions. *Comm. Pure Appl. Math.*, 47(4):405–435, 1994.

[19] Robert V. Kohn and Gilbert Strang. Optimal design and relaxation of variational problems. I. *Comm. Pure Appl. Math.*, 39(1):113–137, 1986.

[20] Robert V. Kohn and Gilbert Strang. Optimal design and relaxation of variational problems. II. *Comm. Pure Appl. Math.*, 39(2):139–182, 1986.

[21] Robert V. Kohn and Gilbert Strang. Optimal design and relaxation of variational problems. III. *Comm. Pure Appl. Math.*, 39(3):353–377, 1986.

[22] Patrick Penzler, Martin Rumpf, and Benedikt Wirth. A phase-field model for compliance shape optimization in nonlinear elasticity. *ESAIM: Control, Optimisation and Calculus of Variations*, 18(1):229–258, 2012.

[23] Roger Temam and Alain Miranville. *Mathematical modeling in continuum mechanics*. Cambridge University Press, Cambridge, second edition, 2005.

[24] Shiwei Zhou and Michael Yu Wang. Multimaterial structural topology optimization with a generalized Cahn–Hilliard model of multiphase transition. *Structural and Multidisciplinary Optimization*, 33:89–111, 2007.